stress values known from extant vertebrates. As these values range from 147 to 392 kPa (ref. 25), a low (mode A) and a high (mode B) estimate of possible muscle force were calculated using the extremes of this range. As stated in the text, the true muscle force values of *Allosaurus* lie within this range—exactly where depends on the animal's physiology. Ventrally directed muscle forces were applied at the attachment sites of all adductor muscles in the correct line of action based upon the anatomy of the lower jaw. Adductor muscles were grouped into three functional units. F_1 = M. adductor posterior; F_2 = M. adductor mandibulae externus group (comprising MAME superficialis, medialis and profundus) and M. pseudotemporalis; F_3 = M. pterygoideus anterior and posterior. The angles between lines of muscle action and the vertical were measured: for F_1, $\alpha = 11°$; for F_2, $\beta = 3°$; for F_3, $\gamma = 62°$.

Bite force calculation

To calculate a static, muscle-driven bite, it is assumed that all muscles are acting in a single parasagittal plane and that the skull is in equilibrium. In these models, *Allosaurus* is biting bilaterally at six teeth in total, the 3rd, 4th and 5th maxillary teeth, left and right sides (see Fig. 1d for details). Thus, three independent equations containing four unknowns are derived. One further assumption must be made; in this case that bite force is vertical. Equations calculate force on one side of the skull only, as forces are equal on both sides. The following equations are used (after refs 26, 27).

$$P\cos\theta + 3B = F_1\cos\alpha + F_2\cos\beta + F_3\cos\gamma \quad (1)$$

$$P\sin\theta + F_1\sin\alpha + F_2\sin\beta = F_3\sin\gamma \quad (2)$$

$$B[\chi_1 + (\chi_1 + \chi_2) + (\chi_1 + \chi_2 + \chi_3)] = F_3d_3 + F_2d_2 + F_1d_1 \quad (3)$$

Where P = condylar force, θ = angle of condylar force, $3B$ = total bite force at three adjacent teeth ($3B/3$ = bite force per tooth). F_1, F_2 and F_3 = adductor muscle force values (low estimate: F_1 = 228.88 N; F_2 = 1173.86 N; F_3 = 1,350.486 N, high estimate: F_1 = 610.3 N; F_2 = 3,130.51 N; F_3 = 3,601.32 N). α, β, γ = angles from vertical for adductor muscle forces (as above). χ_1 = distance from jaw joint to max. 5; χ_2 = distance from max. 5 to max. 4; χ_3 = distance from max. 4 to max. 3; d_1 to d_3 = moment arms for muscle groups F_1 to F_3, respectively; d_1 = 0.0925 m; d_2 = 0.132 m; d_3 = 0.066 m.

Using a high and a low estimate of muscle force leads to a high and a low estimate of bite force and condylar force (Table 1). Again, 'true' values lie within this range. By calculating such a range, assumptions concerning validity of loading parameters may be limited. Low estimate condylar force = 1,957.90 N per condyle; high estimate condylar force = 5,221.46 N per condyle. Angle of condylar forces from the vertical = 33.73°. Comparison with previously published bite force equations[26,27] suggests that experimental error in the calculation of *Allosaurus* bite force is unlikely.

Finite element analysis calculates reaction to the applied load and a defined constraint for each element in turn, to give a composite picture of the mechanical behaviour of the skull (see Fig. 3).

For full descriptions of bite forces for all models featured in this analysis, see Table 1.

Received 24 March; accepted 22 November 2000.

1. Zienkiewicz, O. C. in *The Finite Element Method in Engineering Science* 521 (McGraw-Hill, London, 1971).
2. Ross, C. T. F. in *Finite Element Methods in Engineering Science* 519 (Ellis Horwood, London, 1990).
3. Huiskes, R. & Chao, E. Y. S. A survey of finite element analysis in orthopedic biomechanics: The first decade. *J. Biomechanics* **16,** 385–409 (1983).
4. Huiskes, R. & Hollister, S. J. From structure to process, From organ to cell: Recent developments of FE-analysis in orthopaedic biomechanics. *J. Biomech. Eng., Trans. ASME* **115,** 520–527 (1993).
5. Madsen, J. H. Jr *Allosaurus fragilis*: A Revised Osteology. *Utah Geol. Min. Surv. Bull.* **109,** 1–163 (1976).
6. Paul, G. S. in *Predatory Dinosaurs of The World* 464 (Simon and Schuster, New York, 1988).
7. Farlow, J. O. Speculations about the diet and foraging behaviour of large carnivorous dinosaurs. *Am. Mid. Nat.* **95,** 186-191 (1976a).
8. Farlow, J. O., Brinkman, D. L., Abler, W. L. & Currie, P. J. Size, shape, and serration density of theropod dinosaur lateral teeth. *Mod. Geol.* **16,** 161–198 (1991).
9. Dodson, P., Behrensmeyer, A. K., Bakker, R. T. & McIntosh, J. S. Taphonomy and paleoecology of the dinosaur beds of the Jurassic Morrison Formation. *Paleobiol.* **6,** 208–232 (1980).
10. Molnar, R. E. & Farlow, J. O. in *The Dinosauria* (eds Weishampel, D. B., Dodson, P. & Osmolska, H.) 210–224 (Univ. California Press, Berkeley, 1990).
11. Perez-Moreno, B. P. *et al.* On the presence of *Allosaurus fragilis* (Theropoda: Carnosauria) in the Upper Jurassic of Portugal: first evidence of an intercontinental dinosaur species. *J. Geol. Soc. Lond.* **156,** 449–452 (1999).
12. Erickson, G. M. *et al.* Bite-force estimation for *Tyrannosaurus rex* from tooth-marked bones. *Nature* **382,** 706–708 (1996).
13. Buckland-Wright, J. C. Bone structure and the patterns of force transmission in the cat skull (*Felis catus*). *J. Morph.* **155,** 35–62 (1978).
14. Witmer, L. M. The Evolution of the Antorbital Cavity of Archosaurs: A study in soft-tissue reconstruction in the fossil record with an analysis of the function of pneumaticity. *J. Vert. Paleo. Mem.* **17,** 1–73 (1997).
15. Molnar, R. E. The cranial morphology of *Tyrannosaurus rex. Palaeontographica Abr. A.* **217,** 137–176 (1991).
16. Chin, K., Tokaryk, T. T., Erickson, G. M. & Calk, L. C. A king-sized theropod coprolite. *Nature* **393,** 680–682 (1998).
17. Erickson, G. M. & Olson, K. H. Bite marks attributable to *Tyrannosaurus rex*: preliminary description and implications. *J. Vert. Paleontol.* **16,** 175–178 (1996).
18. Diamond, J. M. in *Principles of Animal Design: The Optimization and Symmorphosis Debate* (eds Weibel, E. R., Taylor, C. R. & Bolis, L.) 21–27 (Cambridge Univ. Press, Cambridge, 1998).
19. Thomason, J. J. & Russell, A. P. Mechanical factors in the evolution of the mammalian secondary palate: a theoretical analysis. *J. Morph.* **189,** 199–213 (1986).
20. Auffenberg, W. *The Behavioural Ecology of the Komodo Monitor.* (Univ. Florida Press, Gainesville, Florida, 1981).
21. Sues, H. D. & Norman, D. B. in *The Dinosauria* (eds Weishampel, D. B., Dodson, P. & Osmolska, H.) 498–509 (Univ. California Press, Berkeley, 1990).
22. Reid, R. E. H. Bone histology of the Cleveland-Lloyd dinosaurs and of dinosaurs in general. *Brig. Young Univ. Geol. Stud.* **41,** 25–71 (1996).
23. Reilly, D. T. & Burstein, A. H. The elastic and ultimate properties of compact bone tissue. *J. Biomech.* **8,** 393–405 (1975).
24. Waters, N. E. in *The Mechanical Properties of Biological Materials* (eds Vincent, J. F. V & Currey, J. D.) 99–135 (Cambridge Univ. Press, Cambridge, 1980).
25. Thomason, J. J., Russell, A. P. & Morgelli, M. Forces of biting, body size, and masticatory muscle tension in the opossum *Didelphis virginiana*. *Can. J. Zool.* **68,** 318–324 (1990).
26. Crompton, A. W. & Hylander, W. L. in *The Ecology and Biology of Mammal Like Reptiles* (eds Hotton, N., Maclean, P. D., Roth, J. J. & Roth, E. C.) 263–282 (Smithsonian Institution Press, Washington DC, 1986).
27. Sinclair, A. G. & Alexander, R. M. Estimated forces exerted by the jaw muscles of some reptiles. *J. Zool.* **213,** 107–115 (1987).
28. Thomason, J. J. Cranial strength in relation to estimated biting forces in some mammals. *Can. J. Zool.* **69,** 2326–2333 (1991).

Acknowledgements

We are grateful to the Bozeman Hospital, Montana, USA, and Picker CT scan Company for CT scanning and file conversion; R. E. H. Reid for advice on dinosaur bone histology and material properties; and M. Harwood for COSMOS/M technical support. J. R. Horner provided access to *Allosaurus fragilis* (MOR 693), C. C. Horner provided use of computing equipment and aided file conversion; P. May Smith assisted with bite force calculations; S. Evans provided crocodile and alligator material for dissection and R. Felix advised on coordinate capture and image production. This work was supported by The Royal Society (D.B.N.), the Natural Environment Research Council, The Department of Earth Sciences and Emmanuel College, Cambridge University and the Cambridge Philosophical Society, and the British Federation of Women Graduates (E.J.R.).

Correspondence and requests for material should be addressed to E.J.R. (email: eray@esc.cam.ac.uk).

Genetic evidence against panmixia in the European eel

Thierry Wirth & Louis Bernatchez

GIROQ, Département de Biologie, Université Laval, Ste-Foy, Québec G1K7P4, Canada

The panmixia hypothesis—that all European eel (*Anguilla anguilla*) migrate to the Sargasso Sea for reproduction and comprise a single, randomly mating population—is widely accepted[1,2]. If true, then this peculiar life history strategy would directly impact the population genetics of this species, and eels from European and north African rivers should belong to the same breeding population through the random dispersal of larvae. To date, the panmixia hypothesis has remained unchallenged: genetic studies realized on eel's mitochondrial DNA failed to detect any genetic structure[3–5]; and a similar lack of structure was found using allozymes[6,7], with the exception of clinal variation imposed by selection[8,9]. Here we have used highly polymorphic genetic markers that provide better resolution[10,11] to investigate genetic structure in European eel. Analysis of seven microsatellite loci among 13 samples from the north Atlantic, the Baltic Sea and the Mediterranean Sea basins reveals that there is global genetic differentiation[12]. Moreover, pairwise Cavalli-Sforza and Edwards'[13] chord distances correlate significantly with coastal geographical distance. This pattern of genetic structure implies

non-random mating and restricted gene flow among eels from different sampled locations, which therefore refute the hypothesis of panmixia. Consequently, the reproductive biology of European eel must be reconsidered[14,15].

Glass eels or fins from adults were collected from different rivers across the European and African coasts (Fig. 1) during spring and autumn 1999. Whole-cell DNA was extracted from 611 individuals and subsequently genotyped at seven mendelian-inherited microsatellite loci. All loci were highly polymorphic in all sampled localities, and the average number of alleles per locus per sample ranged from 12.92 (± 1.44) to 21.23 (± 2.59). Observed and expected mean heterozygosities per sample ranged from 0.835 (± 0.064) and 0.874 (± 0.016) to 0.895 (± 0.054) and 0.934 (± 0.008), respectively. Probability tests of Hardy–Weinberg equilibrium (HWE) using a Markov chain approach (10,000 iterations) were conducted for each of the 13 samples[16]. Seven out of ninety-one cases showed significant departure from HWE after Bonferroni[17] correction ($\alpha = 0.05$, $k = 13$). These departures were not clustered by locus or sample, although the locus Aro121 was involved in four significant tests.

The genetic differentiation based on allelic frequency distribution over all samples was highly significant, and revealed unexpected relationships among the so-called 'panmictic eel' samples ($P = 0.0017$; 10,000 iterations). Population structure among these samples was confirmed by a weak but significant global genetic differentiation (F_{ST}) value of 0.0017 ($P = 0.0014$; 10,000 iterations). Moreover, a pairwise F_{ST} matrix resulted in significant values for south (Mediterranean Sea samples) versus north (Baltic and North Sea) comparisons (6 cases; range 0.003–0.005) and for the Motala river versus other sample comparisons (8 cases; range 0.005–0.012). In the latter comparisons, the smaller sample size for the Motala river ($n = 24$) may be responsible for the significant tests of differentiation.

A principal challenge in situations of slight genetic differentiation is to discriminate between minor but real population structure[18–20] and artefacts due to noise related to sampling errors. Further evidence for population structuring was obtained here by plotting pairwise D_{CE} values against coastal distances (Fig. 2). The Pearson's correlation (r) between the two factors was highly significant ($P < 0.0045$; Mantel test[21]), and the linear regression model explained 21% of the variance between them. This result is therefore consistent with the hypothesis that the European eel exhibits isolation by distance, which implies non-random mating and restricted gene flow among eels from different sampled locations. We also analysed the effect of a single locus on this correlation (r) and the significance (P) of the regression of D_{CE} versus coastal distance by jack-knifing (Table 1). The r values were slightly smaller and the P values slightly less significant than estimated with all seven loci; however, the similar patterns shown by each jack-knifed data set imply that no single locus determined the overall observed positive correlation between D_{CE} and coastal distance. Consequently, selection mediated through gene linkage for particular microsatellite loci could be dismissed. To test whether a bias had been introduced by the inclusion of the Icelandic sample (geographically distant population, putative hybridization with the American eel *A. rostrata*), we redid the analysis without this sample. The results proved to be robust as the correlation between population differentiation and distance remained highly significant ($r = 0.462$ and $P < 0.007$).

To illustrate the putative geographical pattern of genetic differentiation a phenogram was constructed from the D_{CE} pairwise distance matrix using a neighbour-joining[22] algorithm (Fig. 3). We added samples of American eel for the purpose of rooting the tree (our unpublished data). The phenogram grouped the Mediterranean samples in a distinct clade, as well as the North Sea and Baltic sea samples, despite weak bootstrap values. Icelandic eels were intermediate between other *A. anguilla* samples and *Anguilla rostrata*, which is congruent with the genetic status of Icelandic eels for which hybridization with the American eel has been documented[23].

Table 1 Pearson's correlation (r) and the significance (P) of the regression of D_{CE} versus coastal geographical distance in km

Locus excluded*	r	P
Aro 054	0.467	< 0.007
Aro 121	0.298	< 0.028
Ang 114	0.403	< 0.009
Aro 095	0.431	< 0.012
Aro 063	0.533	< 0.014
Ang 151	0.388	< 0.012
Ang 101	0.445	< 0.008
Mean	0.424	
Standard error	0.027	

Based on data sets from which one locus had been excluded by a jack-knifing procedure.

Figure 1 Sampling locations. Locations where glass eels muscle was sampled: Adour, river ($n = 50$); Couesnon, river ($n = 50$); Grand-Lieu, lake ($n = 50$); Minho, river ($n = 50$); Moulonya, oued ($n = 50$); Salses-Leucate, laguna ($n = 41$); Severn, estuary ($n = 50$); Tiber, river ($n = 50$). Locations where yellow eels fin clips were sampled: Arresø, lake ($n = 46$); Elbe, river ($n = 50$); Imsa, river ($n = 50$); Motala, river ($n = 24$); Ölfus, river ($n = 50$).

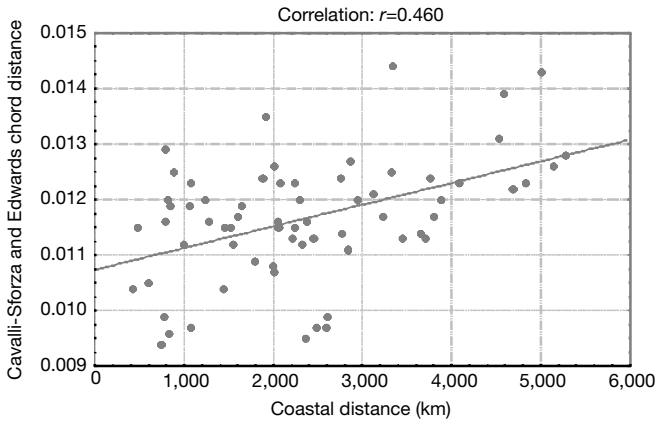

Figure 2 Genetic distance (D_{CE}), based on seven microsatellite loci, versus coastal geographical distances for all possible pairwise combinations of 13 *A. anguilla* samples. A significant positive correlation is observed. Regression analysis: $y = 0.0107 + 4 \times 10^{-7}x$, $r^2 = 0.212$, $P = 0.0045$; Mantel test. A significant positive correlation indicates that samples are spatially genetically structured, with isolation by distance playing an important role. To avoid sample size effects, the Motala sample was not included in this analysis.

Our results thus clearly show that a weak but highly significant genetic structure exists in the European eel, which seems to be related, at least partially, to the maritime units. The panmixia paradigm for this species must therefore be reconsidered. We now have to determine which one of the alternative life history models best explains the observed genetic structure. In a first model, there is a temporal delay between the arrival of adult eels from different latitudes at the common breeding site, which induces higher similarities of synchronic samples breeding together and subsequently larger genetic distances when compared with diachronic samples. North Atlantic individuals may start their reproductive phase earlier in the spring, as the distance to migrate back to the Sargasso Sea is the shortest. This would be followed by North Sea and Baltic Sea individuals and then Mediterranean eels. This temporal allopatry should be reinforced by non-random return of larvae to their parents' ocean basin through active swimming[24] of the leptocephali or through seasonal current changes[25].

In a second model, more than one reproductive area is used by different populations and different currents carry the leptocephali back to their parent's original freshwater habitat. Third, there is only one shared spawning area where assortative mating occurs and larval homing to parents' habitat takes place using an unknown mechanism. Alternatively, homing can take place at later developmental stages involving active juvenile saltwater dispersal.

We concur that the first hypothesis is the most likely, and this does not cast doubt on the observations of Schmidt[1]. The duration of the spawning season (late winter to early summer[1]) might therefore correspond to the arrival of successive waves of reproductive migration. Alternatively, the acceptance of the second hypothesis implies that field observations of Schmidt failed to locate a second or third reproductive area, which seems to be unlikely. Finally, the last hypothesis invokes assortative mating, but the relative important rates of hybridization between American and European eels[23] (5% in Iceland) weakens the efficiency of such processes at the intraspecific level.

More detailed and local ecological and genetic investigations will now be necessary in order to elucidate the exact ecological processes involved in shaping the pattern of population structuring we reported in this study. □

Methods

Genotyping

Genomic DNA was isolated from glass eels muscle or from adults' fin clips according to standard methods[26]. The microsatellite flanking sequences and primers are available on GenBank under the accession numbers AF237896–AF237902. Polymerase chain reactions (PCRs) were performed in duplex or triplex with polymerase and rhodamine-marked primers (Perkin Elmer). Reactions were pooled and alleles belonging to seven different loci were segregated on an ABI377 automated sequencer. The sizes of the fragments were determined in reference to a size standard running in each lane using the software Genescan version 2.1 and Genotyper version 2.0.

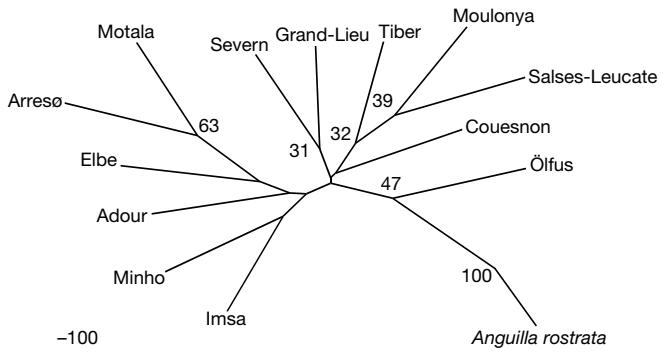

Figure 3 Neighbour-joining phenogram depicting genetic distance relationships based on Cavalli-Sforza and Edward's chord distances among 13 European eel samples. American eel was used as an outgroup. Values on the nodes represent the percentage of bootstrap replicates over loci (n = 2,000) showing the particular nodes, only those with values higher than 30% are reported. Branch lengths are proportional to the genetic distance between the taxa. The scale bar represents a Cavalli-Sforza and Edwards distance (D_{CE}) of 0.0003.

Genetic variability and population genetics parameters

Allelic diversity, genetic variation (observed heterozygosity and unbiased heterozygosity under HWE), deviation from HWE and genetic differentiation were calculated with GENEPOP. Variation of allelic frequencies among samples of *A. anguilla* was assessed by first testing the null hypothesis of homogeneity in allelic distribution by Fisher's exact test using the Markov chain method and then by quantifying the standardized variance in allelic frequencies (θ) as an estimator of F_{ST}, using a described method[12] as implemented in GENETIX 4.0.

Isolation by distance

The relationship of genetic divergence to geographical separation of sites was examined by measuring the Cavalli-Sforza chord distance[13] on the basis of allelic frequencies across the seven loci between each pair of samples. The significance of the relationships between D_{CE} and geographical distances cannot be evaluated using standard regression techniques, as the regression is based on non-independent, pairwise comparisons. We used Mantel's test[21] to assess the significance of the observed correlations. To determine whether one locus contributed disproportionately to the geographic pattern of genetic differentiation, we excluded loci one at a time (jack-knifing over loci) and recalculated the Pearson's correlation (r) of D_{CE} versus geographical distance.

Phylogenetic inference

Cavalli-Sorza and Edwards' chord distance was used to construct a phylogenetic tree using a neighbour-joining algorithm[22]. Support for the tree nodes was assessed by bootstrapping over loci (5,000 iterations). The tree was built using PHYLIP[27] version 3.5c from raw allelic frequencies.

Received 5 June; accepted 4 December 2000.

1. Schmidt, J. The breeding places of the eel. *Smithonian Inst. Ann. Rep.* **1924,** 279–316 (1925).
2. Tesch, F.-W. *The Eel* (Chapman and Hall, London, 1977).
3. Avise, J. C., Helfman, G. S., Saunders, N. C. & Hales, L. S. Mitochondria DNA differentiation in North Atlantic eels: population genetic consequences of an unusual life history pattern. *Proc. Natl Acad. Sci. USA* **83,** 4350–4354 (1986).
4. Sang, T.-Z., Chang, H.-Y., Chen, C.-T. & Hui, C.-F. Population structure of the Japanese eel, *Anguilla japonica*. *Mol. Biol. Evol.* **11,** 250–260 (1994).
5. Lintas, C., Hirano, J. & Archer, S. Genetic variation in the European eel (*Anguilla anguilla*). *Mol. Mar. Biol. Biotech.* **7,** 263–269 (1998).
6. DeLigny, W. & Pantelouris, E. M. Origin of the European eel. *Nature* **246,** 518–519 (1973).
7. Comparini, A., Rizzotti, M. & Rodinó, E. Genetic control and variability of phosphoglucose isomerase (PGI) in eels from the Atlantic ocean and the Mediterranean sea. *Mar. Biol.* **43,** 109–116 (1977).
8. Pantelouris, E. M., Arnason, A. & Tesch, F. W. Genetic variation in the eel. *Genet. Res. Camb.* **16,** 277–284 (1970).
9. Williams, G. C. & Koehn, R. K. in *Evolutionary Genetics of Fishes* (ed. Turner, B. J.) 529–560 (Plenum, New York, 1984).
10. Ruzzante, D. E., Taggart, C. T. Cook, D. A & Goddard, S. V. Genetic differentiation between inshore and offshore Atlantic cod (*Gadus morhua*) of Newfoundland: a test and evidence of temporal stability. *Can. J. Fish. Aquat. Sci.* **54,** 2700–2708 (1998).
11. Shaw, P. W., Turan, C., Wright, J. M., O'Connell, M. & Carvalho, G. R. Microsatellite DNA analysis of population structure in Atlantic herring (*Clupea harengus*), with direct comparison to allozyme and mtDNA RFLP analyses. *Heredity* **83,** 490–499 (1999).
12. Weir, B. S. & Cockerham, C. C. Estimating F-statistics for the analysis of population structure. *Evolution* **38,** 1358–1370 (1984).
13. Cavalli-Sforza, L. L. & Edwards, A. W. F. Phylogenetic analysis: models and estimation procedures. *Am. J. Hum. Genet.* **19,** 233–257 (1967).
14. Castonguay, M., Hodson, P. V., Moriarty, C., Drinkwater, K. F. & Jessop, B. M. Is there a role of ocean environment in American and European eel decline? *Fish. Oceanogr.* **3,** 197–203 (1994).
15. Tsukamoto, K., Nakai, I. & Tesch, W.-V. Do all freshwater eels migrate? *Nature* **396,** 635–636 (1998).
16. Raymond, M. & Rousset, F. GENEPOP (version 1.2): population genetics software for exact tests and ecumenicism. *J. Hered.* **86,** 248–249.
17. Rice, W. R. Analysing tables of statistical tests. *Evolution* **43,** 223–225 (1989).
18. Palumbi, S. R. Genetic divergence, reproductive isolation, and marine speciation. *Annu. Rev. Ecol. Syst.* **25,** 547–572 (1994).
19. Waples, R. S. Separating the wheat from the chaff: patterns of genetic differentiation in high geneflow species. *J. Hered.* **89,** 438–450 (1998).
20. Hutchison, D. W. & Templeton, A. R. Correlation of pairwise genetic and geographic distance measures: inferring the relative influences of gene flow and drift on the distribution of genetic variability. *Evolution* **53,** 1898–1914 (1999).
21. Mantel, N. The detection of disease clustering and a generalized regression approach. *Cancer Res.* **27,** 209–220 (1967).
22. Saitou, N. & Nei, M. The neighbor-joining method: A new method for reconstructing phylogenetic trees. *Mol. Biol. Evol.* **4,** 406–425 (1987).
23. Avise, J. C. *et al.* The evolutionary genetic status of Icelandic eels. *Evolution* **44,** 1254–1262 (1990).
24. Lecomte-Finiger, R. The early life of the European eel. *Nature* **370,** 424 (1994).

25. Marchese, P. J. Variability in the Gulf stream recirculation gyre. *J. Geophys. Res.* **104,** 29549–29560 (1999).
26. Maniatis, T., Fritsch, E. F. & Sambrook, J. *Molecular Cloning. A Laboratory Manual* (Cold Spring Harbor Laboratory Press, Cold Spring Harbor, 1982).
27. Felsenstein, J. PHYLIP (Phylogeny inference package) manual, version 3.5c (Univ. Washington, Seattle, 1993).

Acknowledgements

We are extremely grateful to the following individuals and organizations for providing the samples used in this study: P. Prouzet, G. Adam, M.-N. de Casamajor, S. L. Jónsdóttir, E. Feunteun, P. Lambert, P. Dumont, C. Briand, R. Leconte, A. Crivelli, C. Gazeau, M.-F. Gazerque, D. Fatin, H. Wickström, A. Yahyaoui, C. Antunes, E. Ciccotti, A. Vøllestad, B. Knights, H. Wilkens and the CEMAGREF. We would also like to thank J. Dodson, M. Castonguay, S. Rogers and J. McNeil for helpful comments on an earlier versions of the manuscript. This work is a contribution to the programme of GIROQ.

Correspondence and requests for materials should be addressed to T.W. (e-mail: wirth_t@mpiib-berlin.mpg.de).

Temporal dynamics of a neural solution to the aperture problem in visual area MT of macaque brain

Christopher C. Pack & Richard T. Born

Department of Neurobiology, Harvard Medical School, 220 Longwood Avenue, Boston, Massachusetts 02115, USA

A critical step in the interpretation of the visual world is the integration of the various local motion signals generated by moving objects. This process is complicated by the fact that local velocity measurements can differ depending on contour orientation and spatial position. Specifically, any local motion detector can measure only the component of motion perpendicular to a contour that extends beyond its field of view[1,2]. This "aperture problem"[3] is particularly relevant to direction-selective neurons early in the visual pathways, where small receptive fields permit only a limited view of a moving object. Here we show that neurons in the middle temporal visual area (known as MT or V5) of the macaque brain reveal a dynamic solution to the aperture problem. MT neurons initially respond primarily to the component of motion perpendicular to a contour's orientation, but over a period of approximately 60 ms the responses gradually shift to encode the true stimulus direction, regardless of orientation. We also report a behavioural correlate of these neural responses: the initial velocity of pursuit eye movements deviates in a direction perpendicular to local contour orientation, suggesting that the earliest neural responses influence the oculomotor response.

If a vertically orientated bar moves up and to the right at a constant velocity, small receptive fields positioned along the length of the contour can measure only the rightward component of motion, as the upward component provides no time-varying information (Fig. 1a). In contrast, cells positioned at the endpoints of the contour can measure motion direction accurately. Since direction-selective cells in the primary visual cortex (V1) have extremely small receptive fields, they are constantly faced with this aperture problem. Moreover, they provide directional input to subsequent stages of visual processing, which could perpetuate errors in motion computation. How are these conflicting motion signals ultimately resolved in the visual cortex? A candidate neural substrate for this computation is the middle temporal visual area (MT or V5), where neurons are known to integrate directional responses from V1[4], and are capable of computing motion direction for complex patterns[5–7].

We used the stimulus illustrated in Fig. 1b to measure neuronal responses in MT of alert macaque monkeys to moving contours at different orientations. Each stimulus consisted of a field of small white bars against a dark background. The size of the bar field was matched to each cell's classical receptive field. The length of each bar was always 3°, significantly longer than corresponding receptive fields in V1, but smaller than the excitatory receptive fields in parafoveal and peripheral MT[8]. The use of multiple bars ensured that local motion signals from contours and contour endpoints stimulated the MT receptive fields at each instant. (Additional experiments using single long bars yielded results similar to those reported below, but the bar field had the advantage of providing stimulation that was evenly distributed across the receptive field and relatively constant over time.) On each trial, the angle between motion direction and contour orientation (ϕ in Fig. 1a) was 45°, 90° or 135°, and the stimulus moved in one of eight directions. To separate the selectivity of MT cells to static stimulus orientation[9,10] from their directional responses, the stimulus remained stationary for 240 ms before moving. Because the motion direction and relative orientation, ϕ, both varied in intervals of 45°, the orientation did not predict the subsequent motion direction. The preferred direction (PD) for each cell was computed as a vector average of the stimulus direction weighted by the response to that direction. We recorded data from 60 MT cells from three hemispheres in two adult rhesus monkeys.

Figure 2a shows the results from one MT neuron. The earliest direction-selective responses, which occurred at a latency of approximately 70 ms after the onset of stimulus motion, showed a clear dependence on bar orientation relative to motion direction (ϕ). When the cell was stimulated with a field of bars moving perpendicular to their orientation (ϕ = 90°, red lines), the best responses were obtained for motion down and to the left (PD = 224°). For the ϕ = 45° case (blue lines), the best response occurred for motion to the left (PD = 191°), and in the ϕ = 135° case (green lines), the best response occurred for downward motion (PD = 266°). The effects of contour orientation on the directional responses were highly significant ($P < 0.001$, Watson–Williams test), with the peak response always occurring at the same oblique bar orientation (Fig. 2a). These early responses can best be described as encoding the component of stimulus motion perpendicular to bar orientation. We note that they are not responses to orientation

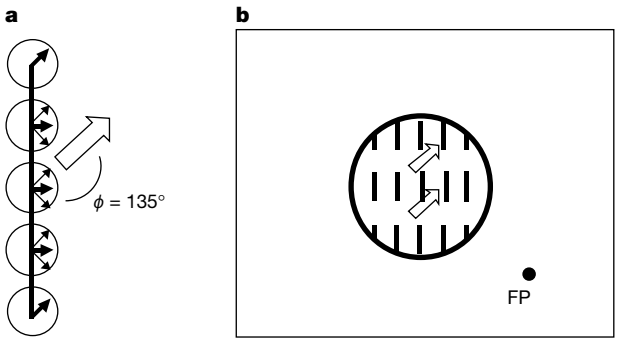

Figure 1 The aperture problem. **a**, Local motion detectors (indicated by the circles) along the contour can only measure motion perpendicular to the contour's orientation. For these detectors, the direction of object motion is ambiguous because any of the physical velocities indicated by the thin black arrows would yield the same motion measurement (thick black arrows). The angle between contour orientation and motion direction, as measured clockwise from the motion direction (white arrow), is referred to as ϕ. **b**, The stimulus used in our experiments. A field of bars moved within a window sized to approximate the classical receptive field (depicted by the large circle) of each cell. FP, fixation point.